

CATALOGED BY DDC
AS AD No. 453421

453421

Report No. 1
Fourth Quarterly Report

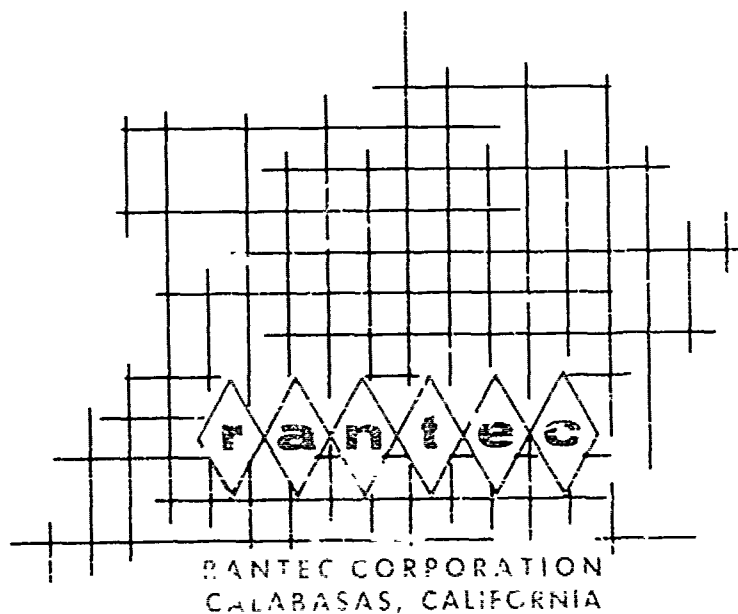
Covering the Period
1 April 1964 to 31 August 1964

**Investigation of
MICROWAVE DIELECTRIC-RESONATOR FILTERS**

Prepared for:
U. S. ARMY ELECTRONICS RESEARCH AND DEVELOPMENT LABORATORY
FORT MONMOUTH, NEW JERSEY

CONTRACT DA 36-039-AMC-02267(E)
TASK NO. 5544-PM-63-91

By: S. B. Cohn and E. N. Torgow



Report No. 1
Fourth Quarterly Report

Covering the Period
1 April 1964 to 31 August 1964

**Investigation of
MICROWAVE DIELECTRIC-RESONATOR FILTERS**

Prepared for:

U. S. ARMY ELECTRONICS RESEARCH AND DEVELOPMENT LABORATORY
FORT MONMOUTH, NEW JERSEY

CONTRACT DA 36-039-AMC-02267(E)
TASK NO 5544-PM-63-91

By: S. B. Cohn and E. N. Torgow

Rantec Project No. 31625

Approved:



SEYMOUR B. COHN, Technical Director

TABLE OF CONTENTS

SECTION	TITLE	PAGE
I	PURPOSE	1
II	ABSTRACT	2
III	CONFERENCES AND PUBLICATIONS	4
IV	FACTUAL DATA	5
	Introduction	5
	Analysis of Coupling Coefficient - Axial Orientation	6
	Resonators Off-Center	17
	Resonator Tilted from the z Axis	17
	Combinations of Misalignments	18
	Comparison of Theoretical and Experimental Coupling Coefficients - Axial Orientation	18
	Coupling of Dielectric Resonators to External Lines	22
	Experimental Investigation of Coupling Techniques	22
	Coupling Between Resonators and Loops	26
V	CONCLUSIONS	30
VI	PROGRAM FOR NEXT INTERVAL	37
VII	LIST OF REFERENCES	38
VIII	IDENTIFICATION OF KEY TECHNICAL PERSONNEL	39
	ASTIA CARDS	40

LIST OF ILLUSTRATIONS

FIGURE	TITLE	PAGE
2-1	Dielectric Disk Resonators Axially Oriented in a Square or Rectangular Cut-Off Waveguide	7
2-2	Coordinate System in Rectangular Waveguide Cross Section	13
3-1	Comparison of Theoretical and Experimental Coupling Coefficient Data for Dielectric Disks in the Axial Orientation Waveguide	19
4-1	Effect of End Couplings on the Response of a Two-Resonator Filter	22
4-2	Shaped Coupling Loop	24
4-3	Two-Resonator Filter Response with Probe End Couplings	25
4-4	Probe Coupling of Dielectric-Resonator Filter . . .	26
4-5	Equivalent Circuit for Loop	27
4-6	External Coupling Loop	30
4-7	Variation of Q_{ex} with Lateral Displacement of Resonator	34

SECTION I

PURPOSE

This program is intended to study the feasibility of high-dielectric-constant materials as resonators in microwave filters, and to obtain design information for such filters. Resonator materials shall be selected that have loss tangents capable of yielding unloaded Q values comparable to that of waveguide cavities. The materials shall have dielectric constants of at least 75 in order that substantial size reductions can be achieved compared to the dimensions of waveguide filters having the same electrical performance.

SECTION II

ABSTRACT

An analysis is given of the coupling coefficient between dielectric-disk resonators arranged axially along the center line of a rectangular metal tube below cutoff. As in the case of the transverse orientation of disk axes treated in the Second and Third Quarterly Reports, a formula is obtained that is reasonably convenient for computation. The formula includes terms for all of the modes excited by the resonators.

In the axial orientation case, the TE_{10} and TE_{01} modes do not contribute to coupling unless the disks are misaligned. The lowest order coupling terms are for the TE_{20} and TE_{02} modes. Formulas for the TE_{10} (and TE_{01}) coupling terms as a function of transverse and angular misalignments are given. These formulas are useful for determining mechanical positioning tolerances necessary in given filter designs.

Experimental coupling-coefficient data are given for the axial orientation. Coupling coefficient versus center-to-center spacing was measured for a pair of dielectric disks in two different sizes of square tubing. Excellent agreement was found with curves computed from the coupling-coefficient formula.

An experimental investigation is described of loop and probe coupling to the end resonators of a series of transverse-oriented coupled dielectric resonators. Principal attention is given in this report to the case of two disks with end couplings adjusted to yield maximally flat response. Asymmetry of the upper and lower stop bands was observed, and was found to be strongly affected by the end coupling elements. Filter response curves are given for various loop and probe designs, showing large differences in the stop-band behavior. With

one coupling configuration using probes, "infinite" rejection peaks appeared in both stop bands. This effect is attributed to direct probe-to-probe coupling bridging the signal path through the coupled dielectric resonators. A formula is derived for the external Q of a disk resonator coupled to a loop, and approximate experimental agreement is shown.

SECTION III
CONFERENCES AND PUBLICATIONS

The period of this program has been extended by one year. By mutual agreement of USAERDL and Rantec Corporation, the fourth quarterly report will cover the investigation interval 1 April to 31 August 1964.

On September 30 and October 1, 1964, a conference was held at Rantec Corporation to discuss work completed during the fourth quarter of the program and plans for the second year. Attending the conference were Mr. E. A. Mariani of USAERDL, and Dr. S. B. Cohn and Mr. E. N. Torgow of Rantec Corporation.

On September 10, 1964, Dr. S. B. Cohn presented a paper covering some of the work on this program at the International Conference on Microwaves, Circuit Theory, and Information Theory, Tokyo, Japan. The title of the paper was "Recent Developments in Microwave Filters and Related Circuits".

SECTION IV

FACTUAL DATA

1. Introduction

The First Quarterly Report¹ discusses the nature of dielectric resonators and describes how such resonators may be used in microwave filters. The introduction to that report should be consulted for background information, and for a discussion of problems to be solved before dielectric resonators can be used in practice.

Earlier reports^{2,3} on this program have been concerned with dielectric disk resonators in a transverse orientation; that is, with their axes transverse to the axis of the surrounding cut-off waveguide. Another arrangement is that of axial orientation, in which the axes of the resonators and waveguide are co-linear. The axial orientation is interesting because it permits a more compact assembly than transverse orientation. Also, it appears to lend itself to practical assembly techniques, especially when round disks are used in a round waveguide.

An analysis is given of coupling between disks in the axial configuration. The treatment is similar to that for transverse orientation. As in the previous analysis, the coupling coefficient is equal to an infinite series of terms for the various excited modes. In this case, the TE_{10} , TE_{01} , and TE_{11} modes in rectangular waveguide do not couple to the resonators. The lowest-order coupling modes are the TE_{20} and TE_{02} . The infinite series in the formula for coupling coefficient converges fairly rapidly and is quite convenient for design purposes. In conjunction with this analysis, measurements of coupling coefficient in the axial orientation were made. The agreement between theory and experiment was remarkably good, generally being within 5 percent.

Several two-resonator band-pass filters (transverse orientation) were described in the Third Quarterly Report. The coupling coefficients, as determined from the measured pass-band responses of the filters, agreed closely with the theoretical and experimental values determined earlier. It was noted, however, that the response characteristics of the dielectric-resonator filters were asymmetric outside of the filter pass bands. The primary source of this asymmetry was ascribed to the characteristics of the input and output coupling elements, which were large, short-circuited loops aligned with their axes parallel to the axes of the dielectric resonators. During the fourth quarter an experimental study was made to determine the factors leading to asymmetric response, and to determine techniques for overcoming this effect. Various loop shapes were investigated, and also probes were used. In addition to achieving improved symmetry, several interesting effects were noticed, such as infinite rejection points appearing in the stop bands under certain conditions. This report also gives an analysis of loop coupling to the end resonators of a filter, and approximate correlation with experimental data. The formula, while not exact, is useful for filter design applications.

2. Analysis of Coupling Coefficient - Axial Orientation

In the Second and Third Quarterly Reports a formula was derived for the coupling coefficient between resonant dielectric disks spaced along the center line of a waveguide for the case of the disk axes in the transverse x direction. Another important case is that of the disk axes in the longitudinal z direction; that is, the axes of the disks and waveguide co-linear, as shown in Figure 2-1. An analysis of this axial configuration in rectangular waveguide is given below, and computed coupling-coefficient values are shown to agree very well with measured points. The case of axial configuration in circular waveguide will be treated in the next report.

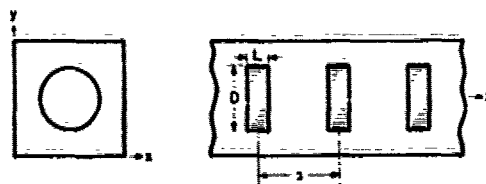


Figure 2-1. Dielectric Disk Resonators Axially Oriented in a Square or Rectangular Cut-Off Waveguide

In the Second Quarterly Report, the following general formula is derived for the coupling coefficient between a pair of identical resonant magnetic dipoles in either a parallel or co-linear configuration:

$$k = \frac{\mu_0 H_2 \cdot m_1}{2W_{m1}} \quad (2-1)$$

where m_1 and W_{m1} are the magnetic dipole moment and stored energy, respectively, of the first dipole when energized at its resonant frequency, and H_2 is the magnetic field at the second dipole due to the first dipole. As discussed previously, the external field of a disk-shaped dielectric resonator ($D/L > 1$) in its lowest-order mode of resonance resembles that of a magnetic dipole directed along the axis of the disk. Thus Eq. 2-1 may be used to compute the coupling coefficient between such resonators.

The analysis will apply to resonators located at any point x, y in the waveguide cross section, but will be particularized for the center-line case ($x = a/2, y = b/2$). For axial orientation, m_1 is in the z -direction. Therefore, the component of H_2 yielding coupling is H_{2z} . Only TE_{mn} modes contribute to coupling, since $H_z = 0$ by definition for TM_{mn} modes.

The Second Quarterly Report² gives formulas for the normalized magnetic field components h_{xmn} and h_{ymn} of the TE_{mn} modes. The corresponding h_{zmn} component is

$$h_{zmn} = \frac{2\pi}{\epsilon_{mn}} \left(\frac{\epsilon_{mn}}{j\omega b \eta_{mn}} \right)^{1/2} \cos\left(\frac{m\pi x}{a}\right) \cos\left(\frac{n\pi y}{b}\right) \quad (2-2)$$

where δ_{mn} is defined as follows

$$\delta_{m0} = 1, \quad m \geq 1$$

$$\delta_{0n} = 1, \quad n \geq 1$$

$$\delta_{mn} = 2, \quad m \neq 1, n \geq 1$$

The other symbols in Eq. 2-2 are defined on pages 9 and 10 of the Second Quarterly Report.

The total field H_{2z} at the second magnetic dipole is expressed in terms of the normalized h_{mn} components as follows (see Second Quarterly Report, page 29)

$$H_{2z} = \sum_{m,n} a_{mn} h_{zmn} e^{-\alpha_{mn} z} \quad (2-3)$$

where a_{mn} are amplitude factors related to the moment of the first magnetic dipole located at $z = 0$. Equations 3-43 and 3-38 of the Second Quarterly Report give

$$a_{mn} = \frac{j\omega\mu_0}{2} h_{zmn} m_{1z} \quad (2-4)$$

It is immediately apparent from Eq. 2-2 that only TE_{mn} modes of even orders contribute to H_z at $x = a/2$ and $y = b/2$. Thus, the significant orders are $m, n = 2, 0; 0, 2; 2, 2; 4, 0; 0, 4; 4, 2; 2, 4; 4, 4$; etc. In the general case of arbitrary location of the resonator in the cross section, TE_{mn} modes of all orders would be significant.

Equations 2-1 and 2-4 assume m_1 to be concentrated at a point. However, in the dielectric resonator, m_1 is actually distributed over

the volume of the disk. Inspection of Eq. 2-2 shows that h_{zmn} has a considerable variation in the plane of the disk, as a result of the $\cos(m\pi x/a) \cos(n\pi y/b)$ factor, especially for the higher modes. Thus, Eqs. 2-1 and 2-4 should be rewritten in this manner,

$$k = \frac{\mu_0}{2W_{m1}} \sum_{m,n} a_{mn} e^{-\alpha_{mn} s} \iiint h_{zmn}(x, y) e^{-\alpha_{mn} z} m'_{1z} dv \quad (2-5)$$

$$a_{mn} = \frac{j\omega\mu_0}{2} \iiint h_{zmn}(x, y) e^{-\alpha_{mn} z} m'_{1z} dv \quad (2-6)$$

where m'_{1z} is the z component of the volume density of magnetic dipole moment, and integration is performed over the disk area and the axial length, $z = -L/2$ to $L/2$. Note that

$$m_{1z} = \iiint m'_{1z} dv$$

When Eqs. 2-5 and 2-6 are combined, one obtains

$$k = \frac{j\omega\mu_0^2}{4W_{m1}} \sum_{m,n} e^{-\alpha_{mn} s} \left[\iiint h_{zmn}(x, y) e^{-\alpha_{mn} z} m'_{1z} dv \right]^2 \quad (2-7)$$

Now consider the fact that m'_{1z} is a symmetrical function of z about the central plane of the disk. Also note that $e^{-\alpha_{mn} z}$ is approximately linear in the $z = -L/2$ to $L/2$ range, when L is small. Hence the volume integral may be replaced by the following surface integral over the central plane of the disk

$$\iint h_{zmn}(x, y) m'_{1z} dS$$

where the area density m'_{1z} is related to m_1 by $m_1 = \iint m'_{1z} dS$. Thus

$$k = \frac{j\omega\mu_0}{4W_{m1}} \sum_{m,n} e^{-\alpha_{mn}s} \left[\iint h_{zmn}(x,y) m'_{1z} dS \right]^2 \quad (2-8)$$

This may be written as

$$k = \frac{j\omega\mu_0}{4W_{m1}} \sum_{m,n} (h_{zmn})^2 K_{mn} e^{-\alpha_{mn}s} \quad (2-9)$$

where h_{zmn} is evaluated at the center of the disk, and K_{mn} is defined as follows:

$$K_{mn} = \left[\frac{\iint h_{zmn}(x,y) m'_{1z} dS}{h_{zmn} \iint m'_{1z} dS} \right]^2 \quad (2-10)$$

$$= \left[\frac{\iint h_{zmn}(x,y) m'_{1z} dS}{h_{zmn} m_1} \right]^2 \quad (2-11)$$

Substitute Eq. 2-2 in Eq. 2-9

$$k = \left(\frac{\mu_0 m_1^2}{2W_{m1}} \right) \left(\frac{4\pi^2}{ab} \right) \sum_{m,n} \frac{\delta_{mn} K_{mn} e^{-\alpha_{mn}s}}{\lambda_{cmn}^2 \sigma_{mn}} \cos^2 \left(\frac{m\pi x}{a} \right) \cos^2 \left(\frac{n\pi y}{b} \right) \quad (2-12)$$

The summation is over $m = 0, 2, 4, 6, \dots$ and $n = 0, 2, 4, 6, \dots$, but does not include the simultaneous combination $m = 0, n = 0$, since the TE_{00} mode does not exist in a metal-walled waveguide.

The first factor in Eq. 2-12, $\mu_0 m_1^2 / 2W_{m1}$, is a function only of the geometry of the dielectric resonator and its ϵ_r value. It is evaluated in the Second Quarterly Report, pages 31 to 33, for the case of the fundamental mode in a disk ($D/L > 1$). To a good approximation,

$$k = \frac{j\omega\mu_0^2}{4W_{m1}} \sum_{m,n} e^{-\alpha_{mn}s} \left[\iint h_{zmn}(x,y) m'_{1z} dS \right]^2 \quad (2-8)$$

This may be written as

$$k = \frac{j\omega\mu_0^2 m_1^2}{4W_{m1}} \sum (h_{zmn})^2 K_{mn} e^{-\alpha_{mn}s} \quad (2-9)$$

where h_{zmn} is evaluated at the center of the disk, and K_{mn} is defined as follows:

$$K_{mn} = \frac{\left[\iint h_{zmn}(x,y) m'_{1z} dS \right]^2}{h_{zmn} \iint m'_{1z} dS} \quad (2-10)$$

$$= \frac{\left[\iint h_{zmn}(x,y) m'_{1z} dS \right]^2}{h_{zmn} m_1} \quad (2-11)$$

Substitute Eq. 2-2 in Eq. 2-9

$$k = \left(\frac{\mu_0 m_1^2}{4W_{m1}} \right) \left(\frac{4\pi^2}{ab} \right) \sum_{m,n} \frac{\delta_{mn} K_{mn} e^{-\alpha_{mn}s}}{\lambda_{cmn}^2 \alpha_{mn}} \cos^2 \left(\frac{m\pi x}{a} \right) \cos^2 \left(\frac{n\pi y}{b} \right) \quad (2-12)$$

The summation is over $m = 0, 2, 4, 6, \dots$ and $n = 0, 2, 4, 6, \dots$, but does not include the simultaneous combination $m = 0, n = 0$, since the TE_{00} mode does not exist in a metal-walled waveguide.

The first factor in Eq. 2-12, $\mu_0 m_1^2 / 4W_{m1}$, is a function only of the geometry of the dielectric resonator and its ϵ_r value. It is evaluated in the Second Quarterly Report, pages 31 to 33, for the case of the fundamental mode in a disk ($D/L > 1$). To a good approximation,

$$\frac{\mu_0 m_1^2}{2W_{m1}} = \frac{0.927 D^4 L \epsilon_r}{\lambda_0^2}, \quad 0.25 \leq L/D \leq 0.7 \quad (2-13)$$

This is within $\pm 2\%$ of a more complicated formula for $\mu_0 m_1^2 / 2W_{m1}$, which also is derived in the Second Quarterly Report. Figure 3-5 of the Second Quarterly Report gives a plot of the error versus L/D , which may be applied to Eq. 2-13 as a correction factor, if desired.

Equation 2-12 will now be particularized for the case of disks located on the central axis of a square waveguide. Thus $b = a$, $x = y = a/2$, and terms of the summation for m,n and n,m are equal. (For example, the TE_{20} and TE_{02} modes yield equal terms.) Remembering the definition of δ_{mn} , we may rewrite Eq. 2-12 as follows.

$$k = \left(\frac{\mu_0 m_1^2}{2W_{m1}} \right) \left(\frac{8\pi^2}{a^2} \right) \left\{ \sum_{\substack{m0 \\ \text{and} \\ mm}} \frac{K_{mn} e^{-\alpha_{mn} s}}{\lambda_{cmn}^2 \alpha_{mn}} + 2 \sum_{\substack{mn \\ (m>n>0)}} \frac{K_{mn} e^{-\alpha_{mn} s}}{\lambda_{cmn}^2 \alpha_{mn}} \right\} \quad (2-14)$$

$m,n = 0, 2, 4, 6, \dots$

Equation 2-10 for K_{mn} will now be evaluated. Since m'_{1z} occurs to the same power in both the numerator and denominator, only a relative value is needed. The magnetic dipole moment per unit area is proportional to the magnetic flux per unit area in the central plane of the disk. That is,

$$m'_{1z} \propto B_{1z} \propto H_{1z}$$

The field distribution in the dielectric disk will be assumed to be that of the second-order solution treated in the First Quarterly Report.

Thus

$$m_{1z} \propto H_{1z} \propto J_0\left(\frac{2p_{01}r}{D}\right), \quad r = 0 \text{ to } D/2 \quad (2-15)$$

where $p_{01} = 2.405$ for the fundamental circular-electric mode. Note that $H_{1z} = 0$ on the circumference of the disk, as is required by the magnetic-wall cylindrical boundary used in the second-order solution.

Substitute Eqs. 2-2 and 2-15 in Eq. 2-10, with h_{zmn} evaluated at the center of the cross section.

$$K_{mn} = \left[\frac{\iint \cos\left(\frac{m\pi x}{a}\right) \cos\left(\frac{n\pi y}{b}\right) J_0\left(\frac{2p_{01}r}{D}\right) r \, dr \, d\theta}{\iint J_0\left(\frac{2p_{01}r}{D}\right) r \, dr \, d\theta} \right]^2 \quad (2-16)$$

$$m, n = 0, 2, 4, 6, \dots$$

The integral in the denominator will be evaluated first.

$$\begin{aligned} I_D &= \int_0^{2\pi} \int_0^{D/2} J_0\left(\frac{2p_{01}r}{D}\right) r \, dr \, d\theta = 2\pi \int_0^{D/2} J_0\left(\frac{2p_{01}r}{D}\right) r \, dr \\ &= \frac{\pi D^2}{2p_{01}^2} J_1(p_{01}) \end{aligned} \quad (2-17)$$

where use was made of⁴

$$\int u J_0(u) \, du = u J_1(u) \quad (2-18)$$

The integral in the numerator will now be treated. As shown in Figure 2-2, the coordinates x and y are related to r and θ by

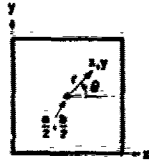


Figure 2-2. Coordinate System in Rectangular Waveguide Cross Section

$$x = \frac{a}{2} + r \cos \theta \quad (2-19)$$

$$y = \frac{b}{2} + r \sin \theta$$

Then, because m and $n = 0, 2, 4, \dots$

$$\cos \frac{m\pi x}{a} \cos \frac{n\pi y}{b} = (-1)^{(m+n)/2} \cos \left(\frac{m\pi r \cos \theta}{a} \right) \cos \left(\frac{n\pi r \sin \theta}{b} \right) \quad (2-20)$$

The factor $(-1)^{(m+n)/2} = \pm 1$ can be ignored, since the integral is squared in Eq. 2-16. Thus the numerator integral may be written

$$I_n = \int_0^{2\pi} \int_0^{D/2} \cos \left(\frac{m\pi r \cos \theta}{a} \right) \cos \left(\frac{n\pi r \sin \theta}{b} \right) J_0 \left(\frac{2p_{01}r}{D} \right) r \, dr \, d\theta \quad (2-21)$$

$$= \int_0^{D/2} \left(\int_0^{2\pi} \cos \left(\frac{m\pi r \cos \theta}{a} \right) \cos \left(\frac{n\pi r \sin \theta}{b} \right) d\theta \right) J_0 \left(\frac{2p_{01}r}{D} \right) r \, dr \quad (2-22)$$

The inner integration can be performed with respect to θ by means of the following formula⁴

$$\int_0^{\pi} \cos(u \sin \theta) \, d\theta = \pi J_0(u) \quad (2-23)$$

First, however, certain substitutions are necessary. Because of the following identity

$$\cos A \cos B = \frac{1}{2} (\cos(A+B) + \cos(A-B)) \quad (2-24)$$

we may write

$$\begin{aligned} & \cos\left(\frac{m\pi r \cos \theta}{a}\right) \cos\left(\frac{n\pi r \sin \theta}{b}\right) \\ &= \frac{1}{2} \cos\left[\pi r \left(\frac{m \cos \theta}{a} + \frac{n \sin \theta}{b}\right)\right] + \frac{1}{2} \cos\left[\pi r \left(\frac{m \cos \theta}{a} - \frac{n \sin \theta}{b}\right)\right] \end{aligned} \quad (2-25)$$

Now let

$$\begin{aligned} \frac{m \cos \theta}{a} \pm \frac{n \sin \theta}{b} &= C \sin(\theta \pm c) \\ &= C \sin c \cos \theta \pm C \cos c \sin \theta \end{aligned} \quad (2-26)$$

Therefore

$$\frac{m}{a} = C \sin c$$

$$\frac{n}{b} = C \cos c$$

and

$$C = \sqrt{\left(\frac{m}{a}\right)^2 + \left(\frac{n}{b}\right)^2} = \frac{2}{c_{mn}} \quad (2-27)$$

Also let

$$\begin{aligned} \theta' &= \theta + c, \quad d\theta' = d\theta \\ \theta'' &= \theta - c, \quad d\theta'' = d\theta \end{aligned} \quad (2-28)$$

The inner integral of Eq. 2-22 can now be given as

$$I_1 = \frac{1}{2} \int_c^{2\pi+c} \cos\left(\frac{2\pi r}{\lambda_{cmn}} \sin \theta'\right) d\theta' + \frac{1}{2} \int_{-c}^{2\pi-c} \cos\left(\frac{2\pi r}{\lambda_{cmn}} \sin \theta''\right) d\theta'' \quad (2-29)$$

These two integrals are equal, since the range of integration in each case is 2π , or one period. Therefore, the inner integral of Eq. 2-22 is equal to

$$I_1 = \int_0^{2\pi} \cos\left(\frac{2\pi r}{\lambda_{cmn}} \sin \theta\right) d\theta \quad (2-30)$$

Equation 2-23 can now be applied, recognizing that $\int_0^\pi = \int_\pi^{2\pi}$. The inner integral is thus equal to

$$I_1 = 2\pi J_0\left(\frac{2\pi r}{\lambda_{cmn}}\right) \quad (2-31)$$

Substitute this in Eq. 2-22 to obtain the numerator integral in the following form:

$$I_N = 2\pi \int_0^{D/2} r J_0\left(\frac{2\pi r}{\lambda_{cmn}}\right) J_0\left(\frac{2p_{01}r}{D}\right) dr \quad (2-32)$$

This can be integrated by means of⁴

$$\int u J_n(au) J_n(bu) du = \frac{au J_n(au) J_{n-1}(bu) - au J_{n-1}(au) J_n(bu)}{a^2 - b^2} \quad (2-33)$$

Let $u = r$, $n = 0$, $J_{-1} = -J_1$, $a = 2\pi/\lambda_{cmn}$, $b = 2p_{01}/D$, and $J_0(p_{01}) = 0$.

Then

$$I_N = \frac{2\pi p_{01} J_0\left(\frac{\pi D}{\lambda_{cmn}}\right) J_1(p_{01})}{\left(\frac{2p_{01}}{D}\right)^2 - \left(\frac{2\pi}{\lambda_{cmn}}\right)^2} \quad (2-34)$$

Substitute Eqs. 2-17 and 2-34 into Eq. 2-16 to obtain

$$K_{mn} = \left[\frac{J_0\left(\frac{\pi D}{\lambda_{cmn}}\right)}{1 - \left(\frac{\pi D}{p_{01} \lambda_{cmn}}\right)^2} \right]^2 \quad (2-35)$$

where $p_{01} = 2.405$.

Finally, coupling-coefficient values may be computed from Eq. 2-14, utilizing Eqs. 2-13, 2-35, and the following:

$$\lambda_{cmn} = \frac{1}{\sqrt{\left(\frac{m}{2a}\right)^2 + \left(\frac{n}{2b}\right)^2}} \quad (2-36)$$

$$\alpha_{mn} = \frac{2\pi}{\lambda_{cmn}} \sqrt{1 - \left(\frac{\lambda_{cmn}}{\lambda}\right)^2} \quad (2-37)$$

In the next section, Eq. 2-14 is used to compute coupling-coefficient-versus-spacing curves for two sets of practical parameters. In each case excellent experimental agreement is found.

Residual TE_{10} -Mode Coupling

The TE_{10} and TE_{01} coupling terms are zero in Eq. 2-14 only if the resonators are perfectly aligned on the central axis of the

waveguide. Weak coupling by these modes can occur if the resonators are slightly off center, or are tilted with respect to the waveguide axis. For close spacings of the misaligned resonators, the $\bar{\text{TE}}_{10}$ and $\bar{\text{TE}}_{01}$ terms will be negligible compared to the higher-order terms in Eq. 2-14, but for wide spacing they will become significant and even predominate, since their attenuation constants are about half that of the $\bar{\text{TE}}_{20}$ and $\bar{\text{TE}}_{02}$ modes.

Two cases of misalignment are considered. These will permit evaluation of the tolerances necessary for Eq. 2-14 to be valid.

a. Resonators Off-Center

Let the resonators be off center by x_1 or $-x_1$. Then

$$x = \frac{a}{2} \pm x_1 \quad (2-38)$$

Equation 2-12 reduces to the following for the $m = 1, n = 0$ term. (The distribution factor K_{10} is assumed equal to 1 for simplicity.)

$$k_{10} = \left(\frac{\mu_0 m_1^2}{2W_{m1}} \right) \frac{\pi^2}{a^3 b} \sin^2 \left(\frac{\pi x_1}{a} \right) \frac{e^{-\alpha_{10} s}}{\alpha_{10}} \quad (2-39)$$

This expression applies to resonators displaced in the same direction. For small displacements of the resonators in opposite directions, it can be shown that the $\bar{\text{TE}}_{10}$ -mode coupling is the negative of the value given in Eq. 2-39.

b. Resonators Tilted from the z Axis

Let the resonator axes be at angle ψ or $-\psi$ with respect to the z-axis in the x, z plane. Then

$$m_{1x} = m_1 \sin \varphi \quad (2-40)$$

The TE_{10} coupling term is obtained as follows from Eq. 2-28 of the Second Quarterly Report².

$$k_{10} = \pm \left(\frac{\mu_0 m_1^2}{2W_{m1}} \right) \frac{\sin^2 \psi}{ab} \alpha_{10} e^{-\alpha_{10} s} \quad (2-41)$$

In this case the + sign applies to tilting in the same direction and the - sign to tilting in opposite directions.

c. Combinations of Misalignments

Coupling can occur if one resonator is displaced and the other tilted, or if combinations of these misalignments occur. Also, coupling can occur if the displacements and tilts are in other than the x-y plane. Equations 2-39 and 2-41 are sufficient, however, for estimating misalignment effects. Other possible cases will be of the same order of magnitude, and hence will not be treated in detail.

3. Comparison of Theoretical and Experimental Coupling Coefficients - Axial Orientation

Coupling measurements were made on a pair of identical dielectric-disk resonators on two sizes of cut-off square waveguide. The configuration is as shown in Figure 2-1. Parameters of the disks are $D = 0.393$ inch, $L = 0.160$ inch, and $\epsilon_r = 97.6$. The waveguide dimensions are 0.625 inch and 0.995 inch. The measurement technique is as discussed in the Second Quarterly Report, pages 34 - 37, except for the axial orientation in the present case.

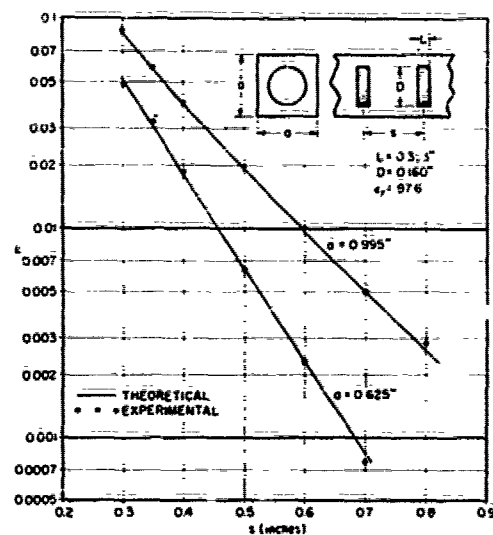


Figure 3-1. Comparison of Theoretical and Experimental Coupling Coefficient Data for Dielectric Disks in the Axial Orientation Waveguide

Figure 3-1 shows theoretical curves and measured coupling-coefficient points plotted versus center-to-center spacing. The theoretical curves are seen to agree with the experimental data extremely well. The various measured points are within 5 percent of theoretical, except for two at large spacing that deviate by about 6 to 8 percent. Since these points are for weak coupling, it is likely that the error is due to residual TE_{1j} coupling. This possibility is supported by calculated values at the end of this section.

The curves in Figure 3-1 were computed from Eq. 2-14 with the aid of Eqs. 2-13, 2-35, 2-36, and 2-37. The parameters for the two curves are as follows:

Curve 1

$$a = b = 0.625 \text{ inch}$$

$$f_0 = 3485 \text{ Mc}$$

$$\mu_0 m_1^2 / 2W_{m1} = 0.0302$$

Curve 2

$$a = b = 0.995 \text{ inch}$$

$$f_0 = 3365 \text{ Mc}$$

$$\mu_0 m_1^2 / 2W_{m1} = 0.0281$$

The above f_0 values are measured center frequencies, and are virtually independent of spacing.

In computing the coupling coefficient, significant mode terms are as indicated by x in the tables that follow. Contribution of terms

for other modes amount to less than 0.5 percent of each coupling-coefficient value.

Curve I

Mode	s, inch						
<u>mn</u>	<u>0.3</u>	<u>0.35</u>	<u>0.4</u>	<u>0.5</u>	<u>0.6</u>	<u>0.7</u>	<u>0.8</u>
20	x	x	x	x	x	x	x
22	x	x	x	x	x	x	x
40	x	x	x				

Curve II

Mode	s, inch						
<u>mn</u>	<u>0.3</u>	<u>0.35</u>	<u>0.4</u>	<u>0.5</u>	<u>0.6</u>	<u>0.7</u>	<u>0.8</u>
20	x	x	x	x	x	x	x
22	x	x	x	x	x	x	x
40	x	x	x	x	x	x	x
42	x	x	x	x	x	x	x
44	x	x	x	x			
60	x	x					
62	x	x					
64	x						

It is clear from these tables that convergence of the infinite series in Eq. 2-14 is rapid except for very close spacing. The more rapid convergence of the series in the case of Curve I results not only from the higher values of the attenuation constants in the smaller waveguide, but also from the fact that K_{mn} decreases more rapidly with m and n when a given resonator is placed in a smaller waveguide.

Misalignment effects will now be computed to determine the effect of TE_{10} -mode coupling in the above cases. First assume the resonators to be displaced by $x_1 = \pm 0.05a$. By Eq. 2-39,

$$k_{10} = \pm 0.00265e^{-2.60s}, \quad (a = b = 0.995 \text{ inch})$$

$$k_{10} = \pm 0.0102e^{-4.70s}, \quad (a = b = 0.625 \text{ inch})$$

At $s = 0.8$ inch, for example,

$$k_{10} = \pm 0.000331, \quad (a = b = 0.995 \text{ inch})$$

$$k_{10} = \pm 0.000237, \quad (a = b = 0.625 \text{ inch})$$

Next assume the resonators to be tilted by $\psi = \pm 5^\circ$. Equation 2-41 gives

$$k_{10} = \pm 0.000562e^{-2.60s}, \quad (a = b = 0.995 \text{ inch})$$

$$k_{10} = \pm 0.00276e^{-4.70s}, \quad (a = b = 0.625 \text{ inch})$$

and at $s = 0.8$ inch,

$$k_{10} = \pm 0.0000703, \quad (a = b = 0.995 \text{ inch})$$

$$k_{10} = \pm 0.0000642, \quad (a = b = 0.625 \text{ inch})$$

It is evident from the above examples that the minor discrepancies at the weak-coupling points in Figure 3-1 are explainable in terms of misalignments. An additional factor is possible accentuation of TE_{10} mode coupling due to the tuning screw utilized in obtaining synchronous tuning of the resonator pair.

4. Coupling of Dielectric Resonators to External Lines

a. Experimental Investigation of Coupling Techniques

The insertion loss response of a two-dielectric-resonator filter, in which the end coupling was accomplished by means of large, short-circuited loops, is shown as Curve I of Figure 4-1. A considerable degree of asymmetry is evident in this curve. Several experiments were conducted during the fourth quarter in order to isolate the cause of the asymmetric response. During the course of these measurements, the distance between resonators was held constant and the input and output couplings were adjusted to yield a maximally flat response.

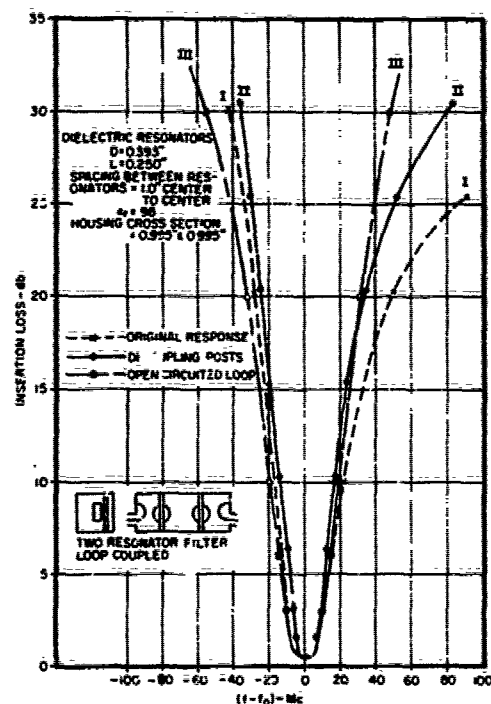


Figure 4-1. Effect of End Couplings on the Response of a Two-Resonator Filter

To determine the degree to which direct coupling between input and output loops affected the response characteristics, two rods were introduced into the filter structure. These rods were located adjacent to each resonator and perpendicular to the plane of the H-field, as shown in Figure 4-1. In this position, the rods have the least effect on the coupling between resonators and on the coupling between each loop and the resonator adjacent to it. Therefore, differences in the filter charac-

teristics observed when the decoupling posts are introduced can be ascribed primarily to the reduction in coupling between the input and output loops. Curve II of Figure 4-1 shows the band pass response of the two resonator filters with the decoupling posts added. A slight narrowing of the pass band was observed, indicating that the posts did have a slight effect upon the coupling between resonators. However, it is evident that the asymmetry was reduced. A third set of data was taken with the decoupling posts removed, but with the loops terminated in an open circuit. The resulting band-pass characteristic, Curve III of Figure 4-1, again exhibited an asymmetry, but the asymmetry is reversed from that observed when the loops were short-circuited. Thus, it appears that in addition to direct coupling, the transmission line effects and the reactances associated with large loops are significant sources of the asymmetries. The effect of these parameters will be examined in greater detail in the following sections.

In addition to the use of a single large loop as a coupling element between a dielectric resonator and its terminating line, several other coupling elements were investigated. A single open-circuited wire parallel to the resonator axis and a small short-circuited wire loop whose axis was perpendicular to the axis of the resonator were placed close to the resonator. The absence of any detectable coupling verified that there were no significant field components orthogonal to the assumed resonator fields. Measurements of the coupling of multi-turn loops (with loop axis parallel to resonator axis) indicated that a two-turn loop coupled slightly more strongly to the resonator than a single-turn loop, but a three-turn loop of approximately the same diameter coupled more weakly to the resonator. It was deduced that the increase in the reactance of the loop more than offset the increase in the induced voltage in the loop (see Para b).

A single-turn loop with the plane of the loop parallel to and partially overlapping the flat surface of a resonator was more

weakly coupled to the resonator than was a non-overlapping loop. This results from the fact that, in the former case, some lines of flux lie completely inside the loop and, therefore, do not contribute to the coupling. More lines of flux will link a loop that is tangent to the cylindrical face of the resonator. Thus, it was observed that partially shaping the loop so that it was in contact with the resonator over a section of the cylinder (see Figure 4-2) increased the coupling. All of the loops

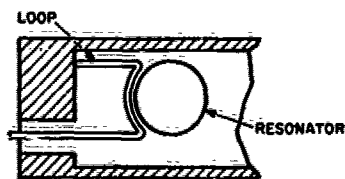


Figure 4-2. Shaped Coupling Loop

used in these experiments were constructed with 0.040 to 0.060 inch diameter wire. Therefore, the reactance of the loops was fairly high. The degree of coupling obtained was fairly weak and indicated that these loops were primarily suited to narrow-band-filter coupling elements.

Simple probe coupling was found to be comparable to loop coupling. A simple wire probe bent to be parallel to the electric field lines in a resonator produced a measured value of external Q of approximately 3000 at a probe-to-resonator center spacing of approximately 0.3 inch. A two resonator filter was constructed with probe end couplings. The performance characteristics of this filter are shown in Figure 4-3. Curve I was obtained when both probes were directed toward the same side of the waveguide axis. When one of the probes was reversed so that the probes were on opposite sides of the waveguide axis, the performance shown by Curve II was obtained. The relative positions of the probes and resonators is shown in Figure 4-4. The difference between the two curves is a direct result of the phase relationship between a signal passing through the filter and a signal coupled directly between the probes. For an even number of resonators, it can be shown that the same phase relationship exists between

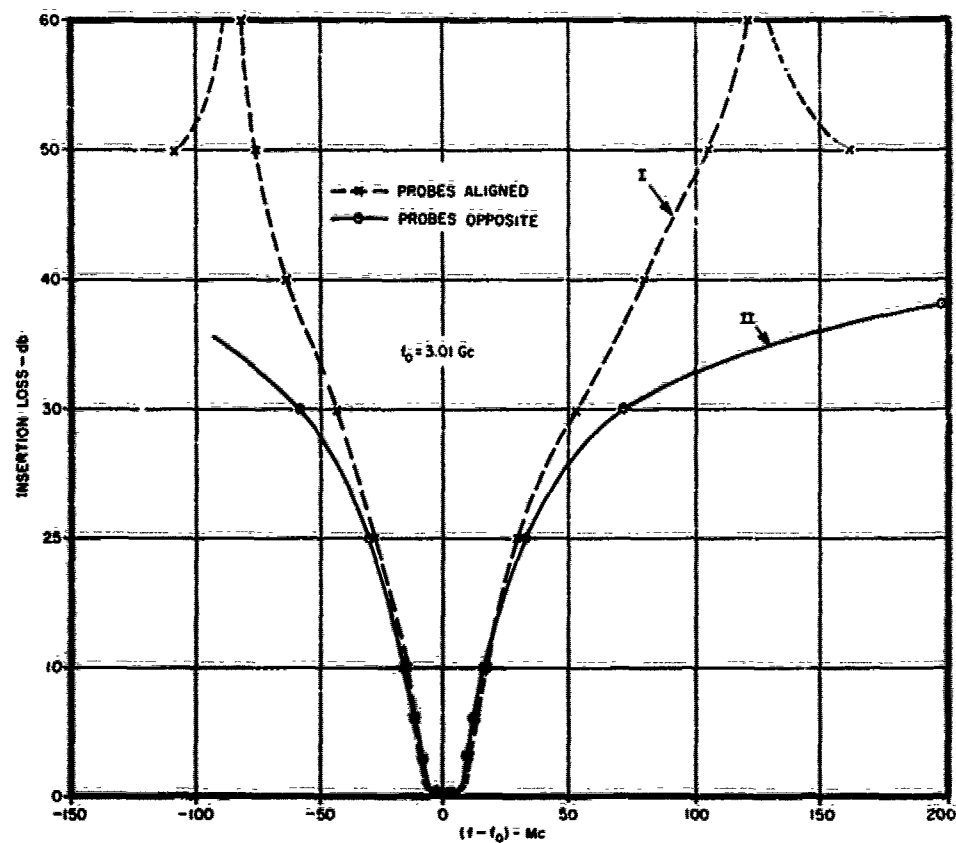
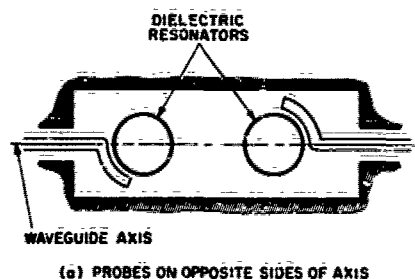
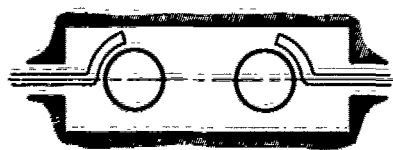


Figure 4-3. Two-Resonator Filter Response with Probe End Couplings

input and output signals above and below the filter pass band. Therefore, probes aligned so that the direct-coupled signal is out of phase with the signal passing through the filter will produce rejection peaks on each side of the pass band. If the orientation of one probe is reversed with respect to the other, the direct-coupled signal is in phase with the filtered signal. In this case, the out-of-band attenuation is reduced on both sides of the pass band. For filters having an odd number of resonators, the phase between input and output signals at frequencies above the pass band differs by 180° from the phase at



(a) PROBES ON OPPOSITE SIDES OF AXIS



(b) PROBES ON SAME SIDE OF AXIS

Figure 4-4. Probe Coupling of Dielectric-Resonator Filter

frequencies below the pass band. In this case, probe-to-probe coupling will cause the rejection to be increased on one side of the pass band and decreased on the other side. The relative orientation of the coupling elements will determine on which side of the pass band the peak will occur. Of course, as the number of resonators is increased the spacing between coupling elements also increases and the direct coupling decreases. Therefore, the amount by which the out-of-band rejection is affected by direct coupling decreases, and the partial cancellation or reinforcement of the rejection characteristic occurs at higher

insertion loss levels.

b. Coupling Between Resonators and Loops

Formulas have been derived for the coupling coefficient between adjacent dielectric resonators inside a waveguide beyond cut-off. The case of cylindrical resonators in rectangular waveguide, where the axes of the resonators are parallel to each other and normal to the axis of the waveguide, was treated in the Second and Third Quarterly Reports. Elsewhere in this report the coupling coefficient between resonators whose axes are aligned with the waveguide axis is derived. The resonant frequency and unloaded Q of dielectric resonators can be readily determined from the dimensions of the resonator and its material properties. Data have also been given for the effects of side walls

upon these parameters. Thus, only one factor remains to be determined, the coupling of the end resonators to the terminating lines, in order to completely specify a dielectric resonator filter.

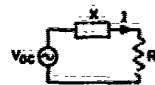
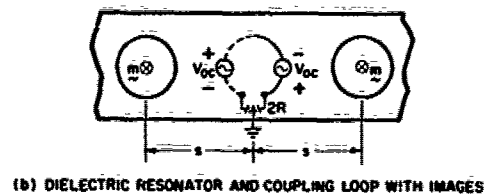
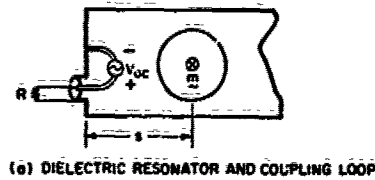


Figure 4-5. Equivalent Circuit for Loop

In the preceding subsections, several different techniques for end coupling dielectric resonators to coaxial lines were described. A formula for loop coupling to a dielectric resonator inside a cut-off rectangular waveguide, and with the resonator axis normal to the waveguide axis, has been derived.

A dielectric resonator loop coupled to a terminating line is shown in Figure 4-5a. If it is assumed that the resonator is energized at its resonant frequency f_0 with a magnetic dipole moment \underline{m}_1 directed out of the page, the

effect of the wall can be determined by taking into account the images of the resonator and loop as shown in Figure 4-5b. The peak open circuited voltage induced in the loop is then given by:

$$2 V_{oc} = 2 \iint_A \frac{d\mathbf{B}}{dt} \cdot d\mathbf{a} \quad (4-1)$$

$$2 V_{oc} = j\omega\mu_0 \iint_A \mathbf{H} \cdot d\mathbf{a} = j\omega\mu H_2 A$$

Where H_2 is the mean value of H normal to the loop due to the dipole moment \underline{m}_1 at a distance s , and A is the area of the loop of Figure 4-5b (twice the area enclosed by the actual loop).

If, as a first approximation, loose coupling is assumed so that the impedance of the resonator seen by the loop at resonance is small and the power dissipated in the resonator can be neglected, then the external Q can be defined by the relation:

$$Q_{ex} = \frac{\omega W_{ml}}{P_d} \quad (4-2)$$

where W_{ml} is the stored energy in the resonator energized by m_l , and P_d is the energy dissipated in the external circuit. Representing the loop and external terminations by a series circuit, Figure 4-5c:

$$P_d = \frac{1}{2} I^2 R = \frac{1}{2} \left| \frac{V_{oc}}{R + jX} \right|^2 R \quad (4-3)$$

where R and X are the real and imaginary parts of the impedance seen at the terminals of the induced voltage generator. The factor of 1/2 reduces the open circuited peak voltage to its RMS value.

Then

$$\begin{aligned} Q_{ex} &= \frac{2\omega W_{ml} (R^2 + X^2)}{\omega^2 \mu_o^2 H_2^2 A^2 R} \\ &= \frac{2W_{ml}}{\mu_o m_l^2} \cdot \frac{(R^2 + X^2)}{\omega \mu_o (H_2/m_l)^2 A^2 R} \end{aligned} \quad (4-4)$$

From Eqs. 3-36, 3-52, of the Second Quarterly Report, and Eq. 2-29 of the Third Quarterly Report, the factors:

$$\bar{F} = \frac{\mu_0 \bar{m}_l^2}{2W_{ml}} \quad (4-5)$$

$$k(s) = \frac{H_2}{m_1} \cdot \bar{F}$$

can be recognized where \bar{F} is a factor that depends only upon the parameters of the resonator and

$$F \approx \frac{0.927D^4 L \epsilon_r}{\lambda_o^2}; \quad 0.25 \leq L/D \leq 0.7 \quad (4-6)$$

for a cylindrical resonator. Furthermore, $k(s)$ is the coupling coefficient between identical resonators, and both experimental and calculated values of $k(s)$ have been given in previous reports for a number of cases.

Thus

$$Q_{ex} = \frac{\bar{F}}{[k(s)]^2} \cdot \frac{R^2 + X^2}{\omega \mu R A^2} \quad (4-7)$$

and as $\omega \lambda_o$ is equal to $2367/\lambda$,

$$Q_{ex} = \frac{\bar{F} \lambda (R^2 + X^2)}{2367 R A^2 [k(s)]^2} \quad (4-8)$$

It can be seen from Eq. 4-8 that the product $Q_{ex} [k(s)]^2$ is independent of the spacing between the resonator and the coupling loop. Therefore it would be expected that the experimentally determined values of $Q_{ex} [k(s)]^2$ would approach this value for loose coupling.

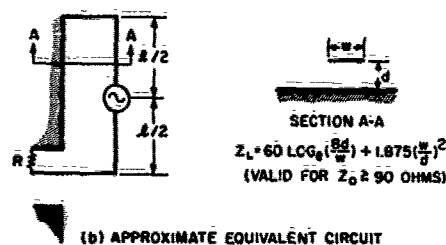
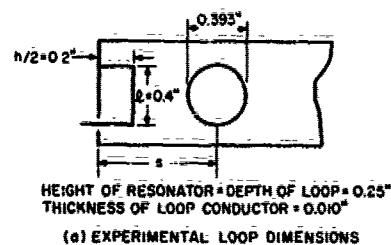


Figure 4-6. External Coupling Loop

given in the Second and Third Quarterly Reports. It can be seen that $Q_{ex}[k(s)]^2$ does indeed approach an asymptote for large spacings.

In order to compare the values of $Q_{ex}[k(s)]^2$ of Table I with that determined by Eq. 4-8, it is necessary that the values of R and X , the real and imaginary parts of the impedance seen by the induced voltage generator be known. Since the fields in the vicinity of the loop are extremely complex, the self inductance cannot be accurately determined. It can be seen from Eq. 4-8 that, if X is comparable in magnitude to, or larger than R , small errors in X can produce large errors in Q_{ex} .

A first approximation assumed that the resistance seen by the voltage generator was the 50-ohm terminating resistance and the reactance was equal to one-half the inductance of a square loop

when proximity effects are minimal. This was confirmed by measurements of Q_{ex} of the rectangular loop of Figure 4-6a coupled to a cylindrical dielectric resonator in a rectangular waveguide beyond cutoff. The results of these measurements are shown in Table I. A correction factor

$$\frac{1}{Q_{ex\ corr}} = \frac{1}{Q_{ex\ meas}} = \frac{1}{Q_u} \quad (4-9)$$

was applied to account for the unloaded Q of the resonator alone. The values of $[k(s)]^2$ are experimentally determined values as

(the actual loop plus its image) in free space. $Q_{ex}[k(s)]^2$ computed on this basis was more than twice the asymptotic value given in Table I.

To more accurately account for the presence of conducting walls in the vicinity of the coupling loop, and for the transmission line effects of a long loop, it was then assumed that the loop was a length of transmission line with a voltage generator in series with the line at its center (See Figure 4-6b). The line was terminated at one end by a short circuit and at the other end by a 50 ohm resistive load. The characteristic impedance of this line was assumed to be that of a flat thin strip above ground. The lengths $l/2$ should be corrected to account for the input and terminating lengths of line. A correction factor should also be applied to the characteristic impedance of the flat strip above ground to take into account the stray capacitance between the strip and the side- and top-walls of the cut-off waveguide. There is no direct analytical method for evaluating these correction factors. The dependence of the factor $Q_{ex}[k(s)]^2$ upon small variations in these parameters can be fairly critical as shown in Table II. The coupling parameter has been computed for a length of line 0.2 inch on each side of the voltage generator and for corrected lengths of 0.25 and 0.3 inch. It can readily be seen that a 0.050 inch variation in length has a significant effect upon the computation of end coupling. Similarly, the last two rows of Table II, which assumed impedance correction factors of 14% and 20%, demonstrates the critical dependence of the coupling upon the impedance parameter.

The assumption was made in the derivation of Eq. 4-6 that the magnetic field across the loop was constant and equal to the field at the center of the loop (including its image). This approximation is more accurate for a circular loop than for the rectangular loop being considered here. If the actual H field variation for a TE_{10} mode in a waveguide beyond cutoff is substituted in Eq. 4-1 the open circuit

TABLE I

Center-to-Center Spacing(s) inch	Q_{ex} meas	Q_{ex} corrected	$[k(s)]^2$	$Q_{\text{ex}}[k(s)]^2$
0.4	85.3	86.3	0.0039	0.338
.46	130.6	133	.0024	.314
.50	203	209	.0016	.334
.57	355	376	.00078	.294
.63	572	626	.000470	.295
.70	1004	1181	.000256	.305
.81	1905	2700	.000011	.296
.97	3933	9940	.00003	.298

$$Q_{\text{ex corrected}} = \frac{1}{\frac{1}{Q_{\text{ex meas}}} - \frac{1}{Q_u}}$$

$$Q_u = 6500$$

TABLE II

$l/2$ inch	Z_L ohms	R ohms	X ohms	$Q_{\text{ex}}[k(s)]^2$	$Q_{\text{ex}}[k(s)]^2$ corrected
0.2	114.2	54.8	69.4	0.318	0.254
.25	114.2	57	88.5	.434	.346
.3	114.2	60.5	108	.564	.451
.3	92.2	59	82	.385	.300
.3	100	60	90	.434	.346

$$f = 3070 \text{ Mc, } \lambda = 3.85 \text{ inches}$$

voltage determined on the basis of a uniform H field distribution must be corrected by the multiplying factor $(\sinh ah/2)/(ah/2)$, where a is the attenuation of the cut-off TE_{10} mode in nepers/unit length and $h/2$ is the height of the loop above the end wall. For the loop of Figure 4-6, the correction factor reduces Q_{ex} by 25%. This correction is shown in the right-hand column of Table II.

It can be assumed that small displacements of the dielectric resonator with respect to the loop, in a direction transverse to the waveguide axis and perpendicular to the axis of the resonator, would cause very small changes in the magnetic field intensity over the loop area. Furthermore, any change in magnetic field intensity would be symmetrical about the axis of the waveguide. Some effects would be expected as a result of the movement of the equivalent induced voltage generator of Figure 4-6b toward, or away from, the short circuited end of the loop. The variation in Q_{ex} for a lateral displacement of the dielectric resonator was computed for an assumed loop impedance of 100 ohms and a loop effective length of $l = 0.6$ inch. The measured values of $k(s)$ given in the Second Quarterly Report were used in these calculations. The calculations are compared to measured values in Figure 4-7, for the case of the dielectric resonator tangent to the loop (center-to-center spacing of 0.4 inch). It can be seen that the actual variation in Q_{ex} is significantly greater than was predicted by the computations. The coupling is considerably weaker when the resonator is displaced toward the input end of the loop and stronger when displaced toward the short-circuited end of the loop.

It can be seen from Figure 4-7, that the stray electric field of a dielectric resonator, energized as shown, produces an electric field between the loop and ground in one direction near the shorted end of the loop and in the opposite direction at the input end of the loop.

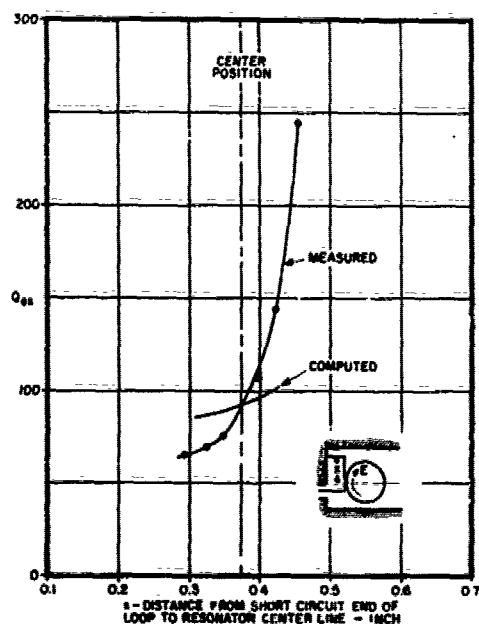


Figure 4-7. Variation of Q_{ex} with Lateral Displacement of Resonator

When the resonator is centered with respect to the loop, these components of electric field are approximately equal and the coupling is entirely due to the magnetic field in the resonator. It can be deduced from the measured data that the electric coupling tends to increase the coupling when the resonator is positioned near the short circuited end of the loop where the maximum magnetic field coupling occurs. When the resonator is displaced away from the shorted end of the loop, where the magnetic field coupling is weaker, the electric field coupling tends to counteract the magnetic field coupling resulting in a significant

decrease in the total coupling between loop and resonator.

Thus it has been demonstrated that the coupling between a dielectric resonator and a loop is critically dependent upon the size, shape, and position of the loop, both with respect to the resonator and with respect to the cut-off waveguide housing. From the steepness of the curves for $k(s)$ as a function of s , it can also be seen that small errors in s will produce substantial errors in the value of Q_{ex} . The error here is greater than in the case of coupling between two resonators, since Q_{ex} is inversely proportional to $[k(s)]^2$. Thus the design of coupling loops for dielectric resonators must be somewhat empirical. This is entirely analogous to the design of loops in cavity-resonator

filters, where some range of adjustment of loop size or position is generally provided, and the adjustment is made such that the prescribed filter performance is achieved.

Design formulas, such as that given by Eq. 4-8 are valuable in that:

1. The approximate size and position of a coupling loop can be determined for a specified degree of coupling; and
2. Variations in coupling as a result of changes in the position or shape of a coupling loop can be predicted. It has also been shown that relatively large coupling loops are required for use with dielectric resonators to realize filters exhibiting fairly narrow (up to approximately 2%) bandwidths.

SECTION V

CONCLUSIONS

The axial arrangement of dielectric disk resonators has several promising properties compared to the previously analyzed transverse arrangement: (1) larger coupling values can be achieved; (2) a given number of resonators can be packed into a smaller volume; and (3) a practical, rugged structure can be readily constructed, especially with circular disks in a cut-off circular waveguide. The coupling-coefficient formula derived for this orientation gives excellent agreement with experimental data.

The problem of loop or probe coupling to the end dielectric resonators of a band-pass filter is too complex for precise analysis. Rough agreement was found between experimental data and a formula for the external Q of an end resonator (transverse orientation) coupled to a loop, but it is clear that empirical adjustment would be necessary in a given filter design. This fact is not unexpected, however, since adjustability of loop or probe couplings is generally necessary in conventional coaxial or waveguide-cavity filters having coaxial terminations. The shape of the stop-band skirts is especially dependent on the nature of the loops or probes. This behavior is partly due to the equivalent circuit of the coupling element and partly due to coupling beyond the adjacent resonator to the second resonator and to the output loop or probe. With probe coupling, "infinite" rejection points could be achieved in both stop bands. This was attributed to a secondary signal path directly between the probes.

SECTION VI

PROGRAM FOR NEXT INTERVAL

The axial-orientation analysis will be extended to the case of a circular cut-off waveguide surrounding the dielectric disks. An approximate formula will be derived for end-loop coupling for this geometry. Experimental data will be obtained for comparison. Applicability of the axial orientation to medium- and wide-band filters will be investigated.

An experimental and theoretical study will be started on band-rejection-filter configurations.

The study of metal-wall proximity effects on Q and f_o of dielectric resonators will be extended and completed.

SECTION VII

LIST OF REFERENCES

1. S. B. Cohn and C. W. Chandler, "Investigation of Microwave Dielectric-Resonator Filters," First Quarterly Report on Contract DA-36-039-AMC-02267(E), 1 July 1963 to 30 September 1963, Rantec Corp., Project No. 31625.
2. S. B. Cohn and K. C. Kelly, "Investigation of Microwave Dielectric-Resonator Filters," Second Quarterly Report on Contract DA-36-039-AMC-02267(E), 1 October 1963 to 31 December 1963, Rantec Corp., Project No. 31625.
3. S. B. Cohn and K. C. Kelly, "Investigation of Microwave Dielectric-Resonator Filters," Third Quarterly Report on Contract DA-36-039-AMC-02267(E), 1 January 1964 to 31 March 1964, Rantec Corp., Project No. 31625.
4. E. Jahnke and F. Emde, "Tables of Functions with Formulae and Curves," p. 145 and p. 150, Dover Publications, New York, 1943.

SECTION VII
IDENTIFICATION OF KEY TECHNICAL PERSONNEL

	Hours
Dr. Seymour B. Cohn Specialist	242
Mr. Eugene N. Torgow Staff Engineer	86
Mr. Charles W. Chandler Senior Engineer	56
Mr. Kenneth C. Kelly Senior Engineer	257
Mr. Richard V. Reed Engineer	513
Mr. Charles M. Oness Engineer	100

AD	DIV Rantec Corporation, Calabasas, California	UNCLASSIFIED	AD	DIV Rantec Corporation, Calabasas, California	UNCLASSIFIED
<p>MICROWAVE DIELECTRIC-RESONATOR FILTERS, by S. B. Cohn and E. N. Torgow, an investigation. Fourth Quarterly Report, 1 April to 31 August 1964, 49p. Incl. illus, tables, 4 refs. (ref. no. 4, proj. 31625) (Contract DA-36-039-AMC-02267(E))</p> <p>An analysis is given of the coupling coefficient between dielectric disk resonators arranged axially along the center line of a rectangular metal tube below cutoff. As in the case of the transverse orientation of disk axes treated in the Second and Third Quarterly Reports, a formula is obtained that is reasonably convenient for computation.</p> <p>In the axial orientation case, the TE₁₀ and TE₀₁ modes do not contribute to coupling unless the disks are misaligned. The lowest order coupling terms are for the TE₂₀ and TE₀₂ modes. Formulas for the TE₁₀ (and TE₀₁) coupling terms as a function of transverse and angular misalignments are given.</p> <p>Experimental coupling-coefficient data are given for the axial orientation. Coupling coefficient versus center-to-center spacing was measured for a pair of dielectric disks in two different sizes of</p>		<p>I. Dielectric-Resonator Filters -- Analyses</p> <p>I. Title: Microwave Dielectric-Resonator Filters</p> <p>II. Cohn, S. B. and Torgow, E. N.</p> <p>III. Rantec Corp., Calabasas, Calif. Contract DA 36-039-AMC-02267(E)</p>		<p>I. Dielectric-Resonator Filters -- Analyses</p> <p>I. Title: Microwave Dielectric-Resonator Filters</p> <p>II. Cohn, S. B. and Torgow, E. N.</p> <p>III. Rantec Corp., Calabasas, Calif. Contract DA 36-039-AMC-02267(E)</p>	
(over)		UNCLASSIFIED		UNCLASSIFIED	
AD	DIV Rantec Corporation, Calabasas, California	UNCLASSIFIED	AD	DIV Rantec Corporation, Calabasas, California	UNCLASSIFIED
<p>MICROWAVE DIELECTRIC-RESONATOR FILTERS, by S. B. Cohn and E. N. Torgow, an investigation. Fourth Quarterly Report, 1 April to 31 August 1964, 49p. Incl. illus, tables, 4 refs. (ref. no. 4, proj. 31625) (Contract DA-36-039-AMC-02267(E))</p> <p>An analysis is given of the coupling coefficient between dielectric disk resonators arranged axially along the center line of a rectangular metal tube below cutoff. As in the case of the transverse orientation of disk axes treated in the Second and Third Quarterly Reports, a formula is obtained that is reasonably convenient for computation.</p> <p>In the axial orientation case, the TE₁₀ and TE₀₁ modes do not contribute to coupling unless the disks are misaligned. The lowest order coupling terms are for the TE₂₀ and TE₀₂ modes. Formulas for the TE₁₀ (and TE₀₁) coupling terms as a function of transverse and angular misalignments are given.</p> <p>Experimental coupling-coefficient data are given for the axial orientation. Coupling coefficient versus center-to-center spacing was measured for a pair of dielectric disks in two different sizes of</p>		<p>I. Dielectric-Resonator Filters -- Analyses</p> <p>I. Title: Microwave Dielectric-Resonator Filters</p> <p>II. Cohn, S. B. and Torgow, E. N.</p> <p>III. Rantec Corp., Calabasas, Calif. Contract DA 36-039-AMC-02267(E)</p>		<p>I. Dielectric-Resonator Filters -- Analyses</p> <p>I. Title: Microwave Dielectric-Resonator Filters</p> <p>II. Cohn, S. B. and Torgow, E. N.</p> <p>III. Rantec Corp., Calabasas, Calif. Contract DA 36-039-AMC-02267(E)</p>	
(over)		UNCLASSIFIED		UNCLASSIFIED	

AD	DIV	UNCLASSIFIED UNITERMS Filters Dielectric-Constant Resonator Cylindrical Rectangular Magnetic-Dipole Measurement Microwave Mode Q Coupling Coefficient Stored Energy Bandpass Loop Coupling Probe Coupling TiO ₂ UNCLASSIFIED	AD	DIV	UNCLASSIFIED UNITERMS Filters Dielectric-Constant Resonator Cylindrical Rectangular Magnetic-Dipole Measurement Microwave Mode Q Coupling Coefficient Stored Energy Bandpass Loop Coupling Probe Coupling TiO ₂ UNCLASSIFIED
AD	DIV	UNCLASSIFIED UNITERMS Filters Dielectric-Constant Resonator Cylindrical Rectangular Magnetic-Dipole Measurement Microwave Mode Q Coupling Coefficient Stored Energy Bandpass Loop Coupling Probe Coupling TiO ₂ UNCLASSIFIED	AD	DIV	UNCLASSIFIED UNITERMS Filters Dielectric-Constant Resonator Cylindrical Rectangular Magnetic-Dipole Measurement Microwave Mode Q Coupling Coefficient Stored Energy Bandpass Loop Coupling Probe Coupling TiO ₂ UNCLASSIFIED

UNITED STATES ARMY ELECTRONICS RESEARCH & DEVELOPMENT LABORATORIES
STANDARD DISTRIBUTION LIST
RESEARCH AND DEVELOPMENT CONTRACT REPORTS

	<u>Copies</u>
OASD (R & E), Room 3E1065, ATTN: Technical Library, The Pentagon, Washington 25, D. C.	1
Chief of Research and Development, OCS, Department of the Army, Washington 25, D. C.	1
Commanding General, U. S. Army Materiel Command ATTN: R & D Directorate, Washington 25, D. C.	1
Commanding General, U. S. Army Electronics Command ATTN: AMSEL-AD, Fort Monmouth, New Jersey	3
Commander, Defense Documentation Center, ATTN: TISIA Cameron Station, Building 5, Alexandria, Virginia 22314	20
Commanding Officer, U. S. Army Combat Developments Command ATTN: CDCMR-E, Fort Belvoir, Virginia	1
Commanding Officer, U. S. Army Combat Developments Command Communications-Electronics Agency, Fort Huachuca, Arizona	1
Chief, U. S. Army Security Agency, Arlington Hall Station Arlington 12, Virginia	2
Deputy President, U. S. Army Security Agency Board Arlington Hall Station, Arlington 12, Virginia	1
Commanding Officer, Harry Diamond Laboratories, Connecticut Avenue & Van Ness St., N. W., Washington 25, D. C.	1
Director, U. S. Naval Research Laboratory, ATTN: Code 2927 Washington 25, D. C.	1
Commanding Officer and Director, U. S. Navy Electronic Laboratory, San Diego 52, California	1
Aeronautical Systems Division, ATTN: ASNNR Wright-Patterson Air Force Base, Ohio 45433	1
Air Force Cambridge Research Laboratories, ATTN: CRZC L. G. Hanscom Field, Bedford, Massachusetts	1
Air Force Cambridge Research Laboratories, ATTN: CRNL-R L. G. Hanscom Field, Bedford, Massachusetts	1

	<u>Copies</u>
114. Electronic Systems Division, ATTN: ESAT L. G. Hanscom Field, Bedford, Massachusetts	1
Rome Air Development Center, ATTN: RAALD Griffiss Air Force Base, New York	1
Advisory Group on Electron Devices, 346 Broadway, 8th Floor, New York, New York 10013	3
AFSC Scientific/Technical Liaison Office, U. S. Naval Air Development Center, Johnsville, Pennsylvania	1
USAEEL Liaison Office, Rome Air Development Center, ATTN: RAOL, Griffiss Air Force Base, New York	1
NASA Representative (SAK/DL), Scientific and Technical Information Facility, P. O. Box 5700 Bethesda, Maryland 20014	2
Commander, U. S. Army Research Office (Durham) Box CM - Duke Station, Durham, North Carolina	1
Director of Procurement & Production Directorate ATTN: AMSEL-PP-E-ASD-5, Fort Monmouth, New Jersey	1
Commanding Officer, U. S. Army Engineer Research & Development Laboratories, ATTN: STINFO Branch Fort Belvoir, Virginia 22060	2
Marine Corps Liaison Office, U. S. Army Electronics Laboratories, Fort Monmouth, New Jersey	1
AFSC Scientific/Technical Liaison Office, U. S. Army Electronics Laboratories, Fort Monmouth, New Jersey	1
Commanding Officer, U. S. Army Electronics Laboratories, ATTN: AMSEL/RD-DR/DE, Fort Monmouth, New Jersey	1
Director, U. S. Army Electronics Laboratories, ATTN: Technical Documents Center, Fort Monmouth, New Jersey	1
Commanding Officer, U. S. Army Electronics Laboratories ATTN: AMSEL-RD-ADO-RHA, Fort Monmouth, New Jersey	1
Commanding Officer, U. S. Army Electronics Research & Development Activity, ATTN: SELWS-A White Sands, New Mexico 88002	1

SUPPLEMENTAL DISTRIBUTION

	<u>Copies</u>
National Bureau of Standards, Engineering Electronics Section ATTN: Mr. Gustave Shapiro, Chief, Washington 25, D. C.	1
Chief, Bureau of Ships, Department of the Navy ATTN: Mr. Cumina, Code 68182, Washington 25, D. C.	1
Commander, Rome Air Development Center, ATTN: Mr. P. Romanelli (RCLRA-2), Griffiss Air Force Base, New York	1
Elec. Engineering Department, University of California at Santa Barbara, ATTN: Dr. G. Matthaei, Santa Barbara, California	1
Physical Electronic Laboratories, 1185 O'Brien Drive, Menlo Park, California, ATTN: Dr. Carter	1
Stanford Research Institute, Menlo Park, California ATTN: Dr. Young	1
Mr. Robert Standley, Antenna Research Facility, I. T. T. Research Institute, Box 205, Geneva, Illinois	1
Mr. Jesse J. Taub, Airborne Instruments Laboratory Deer Park, L. I., New York 11729	1
Professor E. J. Smoke, Rutgers, The State University N. J. Ceramic Research Station, New Brunswick, New Jersey	1
N. J. Gamara, Manager, Antenna R and D Department, Electronic Defense Laboratory, Sylvania Elec. Prods., Inc., P. O. Box 200 Mountain View, California	1
Director, U. S. Army Electronics Laboratories Fort Monmouth, New Jersey	
ATTN: AMSEL-RD-PE (Division Director)	1
ATTN: AMSEL-RD-PE (Dr. E. Roth)	1
ATTN: AMSEL-RD-P (Department Director)	1
ATTN: AMSEL-RD-PEM (Mr. N. Lipetz)	1
ATTN: AMSEL-RD-PEM (Mr. J. Charlton)	1
ATTN: AMSEL-RD-PEM (Mr. E. Mariani)	1